Mechatronics 25 (2015) 18–26

Contents lists available at ScienceDirect

Mechatronics

journal homepage: www.elsevier.com/locate/mechatronics

Dynamic characteristics of planar bending actuator embedded with shape memory alloy

Yong Du, Bo Liu, Min Xu, Erbao Dong, Shiwu Zhang *, Jie Yang

Dept. of Precision Machinery and Precision Instrumentation, University of Science and Technology of China, Hefei, Anhui 230027, China

ARTICLE INFO

Article history:
Received 25 March 2013
Accepted 3 November 2014
Available online 26 November 2014

Keywords:
Planar bending actuator
Shape memory alloy
Dynamic characteristics
Mechanical mode

ABSTRACT

Planar bending actuators embedded with a shape memory alloy (SMA) are a novel type of actuator capable of outputting high bending angle and bending moment. This actuator has a simple structure and high power–weight ratio, which enable it to have wide-ranging applications in the field of biomimetic robots, including biomimetic fish fins and soft robots. However, the existing mechanical model of planar bending actuators embedded with SMA is still quasi-static. Thus, the dynamic characteristics of this kind of actuator cannot be effectively described. Therefore, actuators are difficult to control during the deflection process. To effectively describe this process, a dynamic model of the actuator must be built. This paper aims to identify the dynamic characteristics of the actuator. First, a dynamic model for planar bending actuators embedded with a single SMA wire is established. Second, before SMA wire application, the constitutive characteristics are identified to obtain the necessary parameters for simulation. Third, stable planar bending actuators are fabricated for experiments on characteristics, and then the process flow chart of the planar bending actuator is developed to ensure consistency of the properties of all actuators. Finally, the actuator characteristics obtained experimentally are presented in comparison with those obtained by theoretical simulation. Analysis of the experimental data and simulation results indicates that the planar bending actuator performs better in pulse current heating mode, and that bending angle can be accurately predicted.

1. Introduction

Compared with traditional actuators, actuators embedded with smart materials have a number of advantages, which includes small size, simple structure, and a frequent large output torque [1–3]. Planar bending actuators embedded with smart materials, such as shape memory alloys (SMAs), piezoelectric ceramics, and dielectric rubber, have been widely applied in the field of biomimetic robotics [4,5]. SMA is capable of generating relatively large stress and strain. Thus, actuators embedded with SMA have been applied in micro bionic robot fish [6–8] and bionic caterpillars successfully [9,10].

A range of the bending actuators embedded with SMA wires have been previously studied. Lagoudas studied the one-way shape memory effect of the flexible rods embedded with a single SMA wire. The shape change of the flexible rod was modeled, and the equilibrium between the rod and the SMA linear actuator were derived [11,12]. To drive the rod in two opposite directions and expand the application of the actuator, Blonk and Lagoudas analyzed the actuator embedded with the SMA wire with a two-way shape memory effect [13]. The deflection of the flexible rod was also theoretically modeled by an approximate formula [14–16]. However, in those studies, mechanical models of planar bending actuators embedded with SMA are still quasi-static. The final state of the actuator can be predicted with a quasi-static model. However, the dynamic deflection process of the actuator cannot be determined. In other words, the ultimate deflection angle of the actuator can be deduced based on the quasi-static model, but the deflection angle and the speed of the actuator cannot be obtained at any point, which limits the application. Taking the biomimetic fish fins, which was made using an actuator embedded by a SMA wire, as an example, the dynamic bending process of the fish fins is closely related to the force applied to the fins by water. However, the bending process cannot be obtained with the quasi-static model; only a dynamic model can effectively describe the dynamic bending process of the SMA-driven fins. Yang conducted a study on the control of a SMA-driven actuator, and determined the plot of curvature and time. However, the constitutive equations of the SMA wire were not taken into consideration [17].

* Corresponding author.
E-mail address: swzhang@ustc.edu.cn (S. Zhang).

http://dx.doi.org/10.1016/j.mechatronics.2014.11.001
0957-4158/

The dynamics of bending actuators embedded with SMA wires can be predicted using a set of equations involving the actuator mechanical equation, the SMA material constitutive equation, and the structure thermal transfer equation. To develop a dynamic model, several factors should be considered. First, the inertial force of the substrate should be considered because it associates with the velocity and the acceleration. Second, the control of the actuator should be taken into account, such as different heating control process, because these factors may lead to different results [18,19].

In this study, we constructed a dynamic model of the planar bending actuator, developed a prototype of planar bending actuator, and conducted experiments to verify the theoretical model. The paper is organized as follows: in Section 2, the dynamic theoretical model of the planar bending actuator is constructed; in Section 3, experiments on SMA material are carried out to obtain necessary characteristic parameters for the simulation; in Section 4, the simulation results are presented, effects of various parameters on the performance of the actuator are studied, and the relation between deflection angle and time is investigated; and in Section 5, the prototype of the bending actuator is developed, corresponding experiments are performed to verify those of the simulations, and the output moment is investigated.

2. Modeling the planar bending actuator

The three-dimensional deformations of actuated flexible rods were discussed in detail by Lagoudas and Tadjbakhsh [20]. However, the deflection model of the planar bending actuator is oversimplified under quasi-static conditions. The dynamic mechanical behavior of the actuator is markedly different from those under quasi-static state. Thus, establishing the dynamic mechanical model of the planar bending actuator is necessary for applications.

Fig. 1 shows the configuration of the planar bending actuator with an elastic substrate and an SMA wire. To simplify the model, several assumptions are made: (1) the cross-sectional area of the substrate remains constant in the process of bending; (2) the mass of the SMA wire is much smaller than the substrate, and the inertial force of the SMA wire can be omitted; and (3) the substrate is very thin in the Y-direction and the shear force can be ignored, according to shear lag theory.

2.1. Equilibrium of SMA wire

Based on the equations of the equilibrium of three-dimensional forces and moments, the vector form of the equations of the equilibrium for the SMA wire is

$$\frac{d\boldsymbol{F^a}}{d\boldsymbol{S}_{\mathrm{SMA}}}+\boldsymbol{f^a}=0 \tag{1}$$

where $\boldsymbol{F^a}$ stands for the internal force of the SMA wire that is tangential to its center line; $\boldsymbol{f^a}$ stands for the distributed force, which is applied from the substrate to the SMA wire, and can be decomposed in the tangent direction and the normal direction; and S_{SMA} is the deformed arc length along the actuator. Moreover, $\boldsymbol{F^a}$ and $\boldsymbol{f^a}$ are defined by the following equations:

$$\boldsymbol{F^a}=F^a\boldsymbol{t} \tag{2}$$

$$\boldsymbol{f^a}=f_t^a\boldsymbol{t}+f_n^a\boldsymbol{n} \tag{3}$$

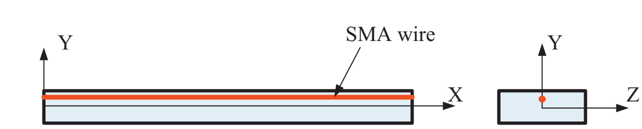

Fig. 1. Sketch of the planar bending actuator with an elastic substrate and an SMA wire.

where $\boldsymbol{t}$ represents the tangent unit vector, and $\boldsymbol{n}$ represents the normal unit vector. The principal normal vector is defined by $\boldsymbol{n} = 1/k \cdot \partial\boldsymbol{t}/\partial S_{\mathrm{SMA}}$, where k is the curvature of the SMA wire. Therefore, the equilibrium equations of the SMA wire can be obtained from the following sets of two equations:

$$\frac{dF^a}{dS_{\mathrm{SMA}}}+f_t^a=0 \tag{4}$$

$$F^a+f_n^a\frac{1}{k}=0 \tag{5}$$

2.2. Equilibrium of the elastic substrate

The mass of the elastic substrate is much larger than the SMA wire. Therefore, the inertial force of the substrate cannot be ignored. In the model, the position vector of any cross-section of the elastic substrate is denoted as $\mathbf{r}(S,t)$. Conservation of linear and angular momentum can deduce the equations of motion. The balance of forces and couples at each cross-section yields the following equations of motion:

$$\frac{d\boldsymbol{F}}{d\boldsymbol{S}}+\boldsymbol{f}=\rho_0 A\boldsymbol{r}_{tt} \tag{6}$$

$$\frac{d\boldsymbol{M}}{dS}+\frac{d\boldsymbol{X}}{dS}\times\boldsymbol{F}+\boldsymbol{m}=\rho_0\boldsymbol{I}\boldsymbol{\theta}_{tt} \tag{7}$$

where ρ_0 is the mass density of the substrate; A is the cross-sectional area of the substrate; $\boldsymbol{F}$ is the resultant force vector of the substrate; and $\boldsymbol{f}$ is the distributed forces acted from the SMA line actuator. The steady motion consists of the translation of the substrate along its tangent at a constant speed, denoted as $v(t)$ and the speed of any point along the normal direction to the center line of the substrate, denoted as $v(n)$. The inertial acceleration $\boldsymbol{r}_{tt}$ induced by this motion is given by:

$$\boldsymbol{r}_t=v(t)\boldsymbol{t}+v(n)\boldsymbol{n},\boldsymbol{r}_{tt}=\frac{\partial v(t)}{\partial t}\boldsymbol{t}+kv^2(t)\boldsymbol{n}+\frac{\partial v(n)}{\partial t}\boldsymbol{n}-kv(n)v(t)\boldsymbol{t}$$

The value of $v(t)$ is observed to be very small, thereby allowing $\boldsymbol{r}_{tt}$ to be simplified as $\boldsymbol{r}_{tt} = \partial v(n)/\partial t \cdot \boldsymbol{n}$. $\boldsymbol{M}$ is the resultant moment vector of the substrate; $\boldsymbol{X}$ is the position vector of the deformed centroid line of the substrate; and $d\boldsymbol{X}/dS = (1 + e)\boldsymbol{e}_y$, $\boldsymbol{m} = \boldsymbol{d} \times \boldsymbol{f}$ is the resultant moment vectors of the SMA line actuator.

The planar bending actuator embedded with SMA wires only deflects in two-dimensional plane. Thus, $\boldsymbol{F}$ and $\boldsymbol{f}$ can be simplified as the following equation:

$$\boldsymbol{F}=F_x\boldsymbol{e}_x+F_y\boldsymbol{e}_y \tag{8}$$

$$\boldsymbol{f}=f_x\boldsymbol{e}_x+f_y\boldsymbol{e}_y \tag{9}$$

The curvatures of the deformed shape of the substrate and the deformed body triad are expressed as follows:

$$\frac{d\boldsymbol{e}_x}{dS}=k_y\boldsymbol{e}_z-k_z\boldsymbol{e}_y \tag{10}$$

$$\frac{d\boldsymbol{e}_y}{dS}=k_z\boldsymbol{e}_x-k_x\boldsymbol{e}_z \tag{11}$$

The equilibrium equations of the elastic substrate can then be resolved as follows:

$$\frac{dF_x}{dS}+k_zF_y+f_x=0 \tag{12}$$

$$\frac{dF_y}{dS}-k_zF_x+f_y=0 \tag{13}$$

Notably, $\ddot{\boldsymbol{\theta}} = \ddot{\theta}\boldsymbol{e}_z$, such that the moment balance equations of the elastic substrate can be deduced from the following equation:

$$\frac{dM_z}{dS} + (1+e)F_y - df_x = \rho_0 I \frac{\partial^2 \theta}{\partial t^2} \tag{14}$$

In the two-dimensional plane coordinate system, $\boldsymbol{t} = \boldsymbol{e}_x$, $\boldsymbol{n} = \boldsymbol{e}_y$, $f = -dS_{SMA}/dS \cdot f^a$, and $dS_{SMA}/dS = 1$, which results in the following equations:

$$f_x = -f_t^a \tag{15}$$

$$f_y = -f_n^a \tag{16}$$

The equilibrium equations for the substrate and the SMA wire can then be simplified and expressed by the following equations:

$$\frac{dF_x}{dS} - kF_y + \frac{dF^a}{dS} = 0 \tag{17}$$

$$\frac{dF_y}{dS} + kF_x + kF^a = \rho_0 A \frac{\partial v(n)}{\partial t} \tag{18}$$

$$\frac{dM_z}{dS} + (1+e)F_y - d\frac{dF^a}{dS} = \rho_0 I \frac{\partial^2 \theta}{\partial t^2} \tag{19}$$

2.3. Constitutive equation of the SMA wire

In this section, the relation between the SMA temperature, stress, and strain is described according to the Tanaka model [21]. The constitutive model of the SMA can be used in the differential expression as follows:

$$\dot{\boldsymbol{\sigma}} = D\dot{\boldsymbol{\varepsilon}} + \Theta\dot{\boldsymbol{T}} + \Omega\dot{\xi} \tag{20}$$

where σ is the stress of the SMA wire and Θ is the thermal elastic tensor; D is the elastic modulus of the SMA wire in any temperature; and Ω is the phase change tensor. However, if the rate of change of the temperature is not rapid, the thermal elastic tensor can be ignored and the relationship between them is reduced to the following:

$$D = E_A + \xi(E_M - E_A) \tag{21}$$

$$\Omega = -\varepsilon_{\mathrm{SMA}} D \tag{22}$$

where E_A represents the elastic modulus of Austenite, E_M represents the elastic modulus of Martensitic, ξ is the Martensitic volume fraction, D is $\varepsilon_{\mathrm{SMA}}$ is the maximum residual strain.

A bending sketch of the actuator is shown in Fig. 2 to obtain ε, where d is the distance between the axis of the SMA wire (the cyan line) and the axis of the elastic substrate (the magenta line), and r is the radius of the arc. According to geometrical relationship, following equation can be obtained:

$$\frac{l(1+e)}{r+d} = \frac{l(1-\varepsilon)}{r} \tag{23}$$

where e is the elongation of the elastic substrate; ε is the strain of the SMA wire; and l is the original length of the substrate which is equal to the original length of the SMA wire. The curvature of the central axis of the elastic substrate is k, which is the reciprocal of $r + d$, and the above formula can be simplified as follows:

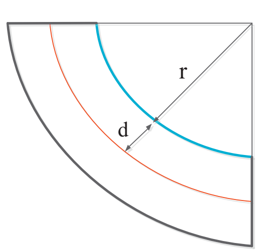

Fig. 2. Bending sketch.

$$\varepsilon = e - kd - ekd \tag{24}$$

The internal force of the SMA line actuator is given by:

$$F^a = DA^a(e - kd - ekd - \varepsilon_{SMA}(\xi - 1)) \tag{25}$$

From the above equation, we found out that the driving force of the SMA line actuator has a direct relationship with the Martensitic volume fraction. To accurately depict the relationship between the Martensitic volume fraction and the temperature, Liang and Rogers [22] used the cosine functions to describe their relevance based on the phenomenological analysis method.

The Martensitic volume fraction in the process of Martensitic transformation is expressed as

$$\xi = \frac{1-\xi_A}{2}\cos[a_M(T - M_f) + b_M\sigma] + \frac{1+\xi_A}{2}$$
$$M_{\sigma f} \leqslant T \leqslant M_{\sigma s} \tag{26}$$

By contrast, the Martensitic volume fraction in the process of reverse Martensitic transformation is expressed as

$$\xi = \frac{\xi_M}{2}\cos[a_A(T - A_s) + b_A\sigma] + \frac{\xi_M}{2}$$
$$A_{\sigma s} \leqslant T \leqslant A_{\sigma f} \tag{27}$$

ξ_A and ξ_M describe the process of $A \to M$ and the reverse Martensitic transformation $M \to A$, respectively, at the beginning of the Martensitic volume fraction in the Martensitic transformation process. M represents the SMA wire in the martensitic phase, and A means the SMA wire in the austenite phase. The influence of temperature on the phase transition is described by a_M and a_A, whereas the influence of stress on the phase transition stress of the phase transition is described by constants b_M and b_A. These constants are defined as the following:

$$a_M = \frac{\pi}{M_s - M_f} \tag{28}$$

$$a_A = \frac{\pi}{A_f - A_s} \tag{29}$$

$$b_M = -\frac{a_M}{C_M} \tag{30}$$

$$b_A = -\frac{a_A}{C_A} \tag{31}$$

C_A and C_M are constants which represent the influence of stress on the phase transition temperature, and can be determined from the slope of the phase transition line in the SMA stress–temperature phase diagram.

2.4. Thermodynamic equation of the SMA wire

The relationship between the temperature and the heating voltage of the SMA wire can be obtained according to the thermal equilibrium of the SMA wire and environment. The energy delivered to the wire by the electrical voltage must equal the change in internal heat energy of the SMA wire plus the energy transferred to environment by natural convection. Therefore, the heat balance equation of the SMA wire is given as

$$\frac{V^2}{r_{\mathrm{SMA}}} = mc_p\left(\frac{dT}{dt}\right) + HA(T - T_0) \tag{32}$$

where m is the mass of the SMA wire; c_p is the specific heat of the SMA wire; T is the instantaneous temperature of the SMA wire; T_0 is the temperature of the environment; r_{SMA} is the resistance of the SMA wire; V is the heating voltage; H is the average heat transfer coefficient between the SMA wire and environment; and A is the surface area of the SMA wire.

A combination of the dynamic mechanical model of the SMA wire and elastic substrate with the constitutive and thermodynamic equations of the SMA wire allows the calculation of the bending speed and the angle of the actuator at any moment.

As the driving part of the actuator, the performance of the SMA wire has a critical influence on the actuator. However, there is much variation among the properties of different SMA wires because of the Ni–Ti ratio and the treatment process, to name a few factors. Thus, the characteristics of the SMA wires are studied prior through several experiments to obtain several necessary parameters about SMA wires.

3. Experiment on the characteristics of SMA wires

The characteristics of the SMA wire directly influence the properties of the planar bending actuator. Experiments on characteristics of SMA wires need to be performed to obtain necessary parameters. Ni–Ti (50.6%) SMA wires with diameter of 0.15 mm were used in the experiment. Phase transition temperatures were firs measured using differential scanning calorimetry (DSC, Q2000, TA Instruments, America). As shown in Fig. 3, the phase transition temperature of the SMA wire can be calculated from the DSC graph, and are listed in Table 1.

The relationship between the phase transition temperature and the stress can be expressed as follows:

$$M_{\sigma s} = M_s + \frac{\sigma}{C_M} \tag{33}$$

$$M_{\sigma f} = M_f + \frac{\sigma}{C_M} \tag{34}$$

$$A_{\sigma s} = A_s + \frac{\sigma}{C_A} \tag{35}$$

$$A_{\sigma f} = A_f + \frac{\sigma}{C_A} \tag{36}$$

The above equations present that the phase transition temperature possesses a linear relationship to the stress. A dynamic mechanical thermal analyzer (DMA, DMTAQ800, TA Instruments, America) was used to test the behavior of SMA wires under different stresses. The relationships between the temperature and the strain under different stresses are displayed in Fig. 4. Results showed that both the maximum strain and the phase transition temperature increase with increasing stress. The phase transition temperature is obtained by the tangent-intersection method as shown in Fig. 5 and results are shown in Fig. 6. The influence of stress on the phase transition temperature are represented by C_A and C_M, which can be calculated from the figure by curve fitting, $C_A = 11.23$ N/K mm^2, $C_M = 6.33$ N/K mm^2.

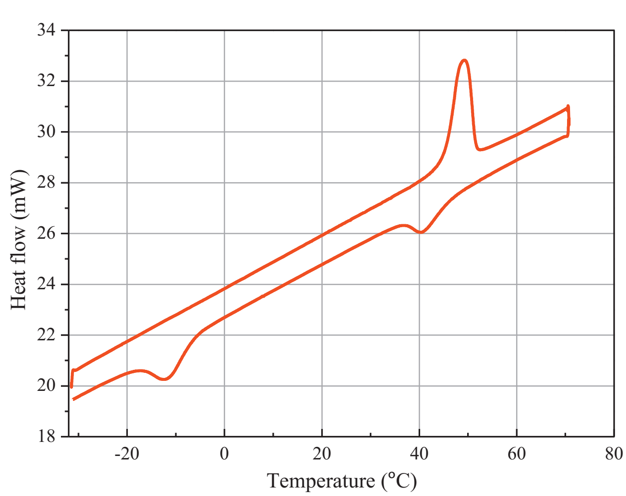

Fig. 3. DSC curve for phase transition temperature measurements.

Table 1
Phase-transition temperature and thermal enthalpy.

Samples	Phase-transition temperature (°C)		Phase-transition thermal enthalpy (J/g)	
SMA wire 0.15 mm	A_s	45.6	$\Delta H_{M\text{-}A}$	16.2
	A_f	51.6		
	R_s	44.6	$\Delta H_{A\text{-}R}$	−3.97
	R_f	37.2		
	M_s	−6.8	$\Delta H_{R\text{-}M}$	−7.13
	M_f	−17.3		

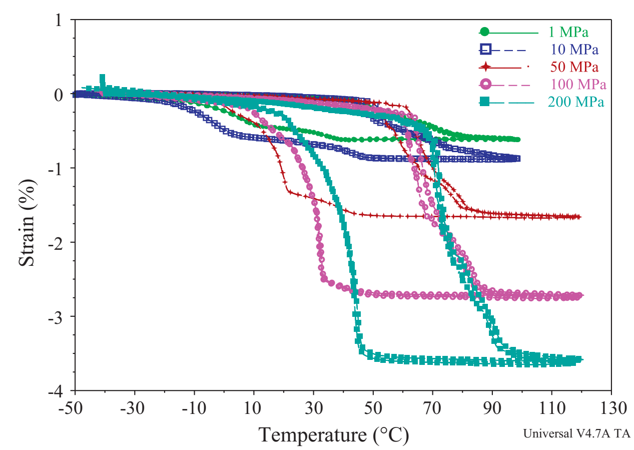

Fig. 4. DMA curves with different stress.

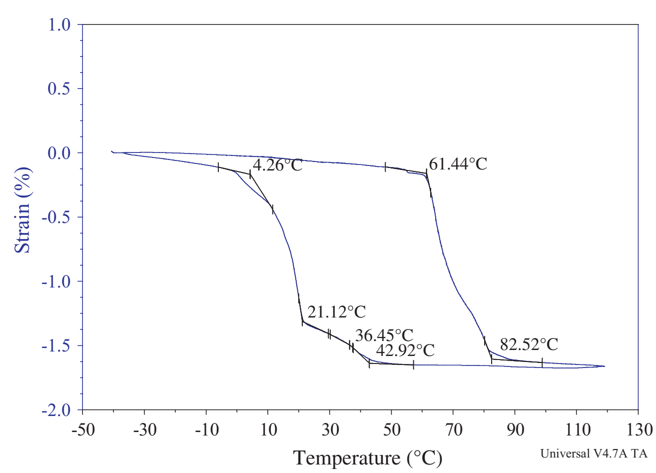

Fig. 5. DMA measuring curve for phase transition measurements.

4. Simulation on the planar bending actuator

The numerical simulation was conducted to analyze the effect of various parameters on the performance of the actuator. The

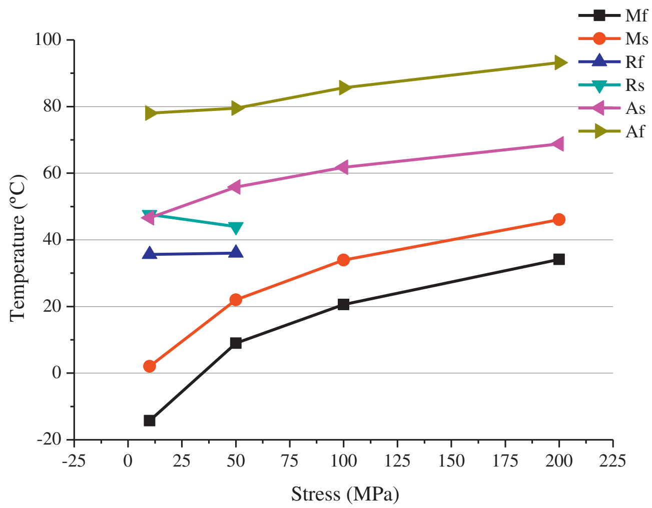

Fig. 6. Analysis of phase transition temperatures with different stresses.

parameters used for simulation are summarized in Table 2. Among the SMA wire parameters, the convective heat transfer coefficient is critically important compared with other parameters because it determines the steady-state temperature of the SMA wire in response to the current. The heat transfer coefficient of a horizontal cylinder of wire of 2 cm diameter in water is 890 $Wm^{-2}\,{}^{\circ}C^{-1}$ [23]. In this prototype, the SMA wire is covered by a silicone membrane. The silicone membrane is likely to act as a heat sink, which increases the heat transfer coefficient. Assuming the silicone membrane over the whole length of the SMA wire has the same heat transfer coefficient, we could expect that the heat transfer coefficient of the SMA wire in this prototype will be reduced to approximate the heat transfer coefficient between the SMA wire and air. The heat transfer coefficient in the setup will be more than the heat transfer coefficient of a horizontal cylinder of 2 cm diameter in water. The heat transfer coefficient from the SMA wire to air is 1200 $Wm^{-2}\,{}^{\circ}C^{-1}$; thus, the heat transfer coefficient in the simulation is set as 1000 $Wm^{-2}\,{}^{\circ}C^{-1}$.

First, the relationship between the deflection angle and the maximum residual strain, or the pre-stretching rate, was analyzed. As shown in Fig. 7, the deflection angle increases with heating voltage at a constant maximum residual strain. Moreover, at a constant heating voltage, an increase in the residual strain leads to a decrease in the deflection angle. One explanation is that more residual strain indicates a larger stress, leading to a higher phase transition temperature and more energy for the transformation. As a rule of thumb, the maximum residual strain should not be very large, such that the value of the maximum residual strain was chosen to be 4% in the later simulation and experiment.

The relationship between the diameter of the SMA wire and the deflection angle was also investigated. The SMA wire provides the driving force for the planar bending actuator. The larger the diameter of the SMA wire is, the bigger the actuator force it can provide. As presented in Fig. 8, at a constant heating voltage, a larger diameter of the SMA wire results in a larger deflection angle. In the experiments, a maximum deflection angle can be obtained when the diameter of the SMA wire is 0.4 mm. A larger diameter of the SMA wire, which could provide a greater force, allows a

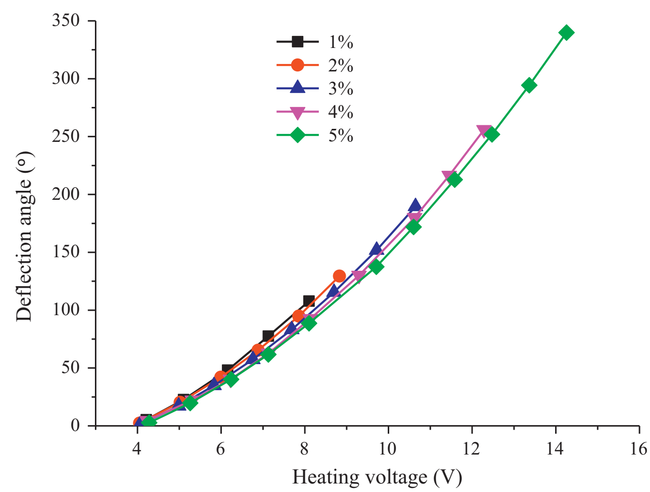

Fig. 7. Relationship between the deflection angle and the maximum residual strain. (The diameter of the SMA wires was 0.2 mm, the heating voltage was from 3 to 16 V).

Table 2
List of simulation parameters.

Parameter	Label	Unit	Values
Radius of SMA wire	r	mm	0.075–0.2
Density of SMA wire	ρ	g/mm^3	0.00647
Length of SMA wire	l_{SMA}	mm	120
Average heat transfer coefficient between the SMA wire and external environment	H	$Wm^{-2}\,{}^{\circ}C^{-1}$	1000
Specific heat capacity of SMA wire	c_p	J/g K	0.6
Ambient temperature	T_0	°C	24
Phase transition starting temperature	M_s	°C	−6.8
Phase transition finishing temperature	M_f	°C	−17.3
Inverse phase transition starting temperatures	A_s	°C	45.6
Inverse phase transition finishing temperatures	A_f	°C	51.6
Martensitic stress influence coefficient	C_M	$N/K\,mm^2$	6.33
Austenitic stress influence coefficient	C_A	$N/K\,mm^2$	11.23
The influence of temperature on the Martensitic phase transition	a_M	N/A	0.2992
The influence of temperature on the austenitic phase transition	a_A	N/A	0.5236
The influence of phase transition stress on the Martensitic phase transition	b_M	N/A	−0.04727
The influence of phase transition stress on the austenitic phase transition	b_A	N/A	−0.04663
The elastic modulus of SMA in austenitic	E_A	N/mm^2	83,300
The elastic modulus of SMA in martensitic	E_M	N/mm^2	40,000
The width of the substrate	b	mm	20
The thickness of the substrate	h	mm	0.32
The length of the substrate	l	mm	60
The elastic modulus of substrate	E	N/mm^2	2410
The moment of inertia of substrate	I	N/A	0.05461

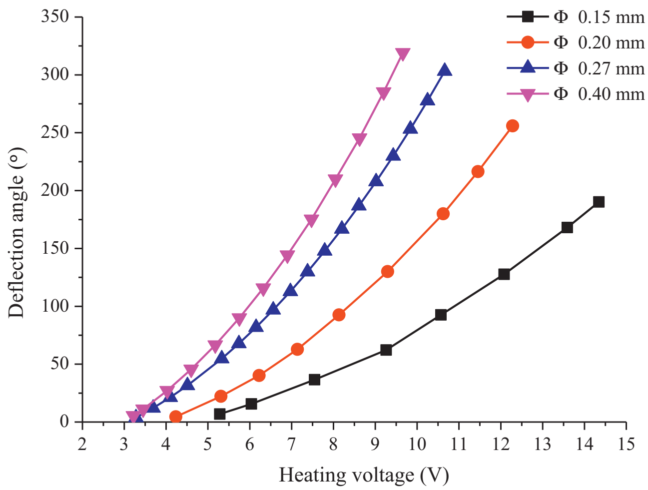

Fig. 8. Relationship between the diameter of the SMA wire and the deflection angle. (The maximum residual strain of the SMA wire was chosen to be 4%, and the heating voltage used was from 3 to 16 V).

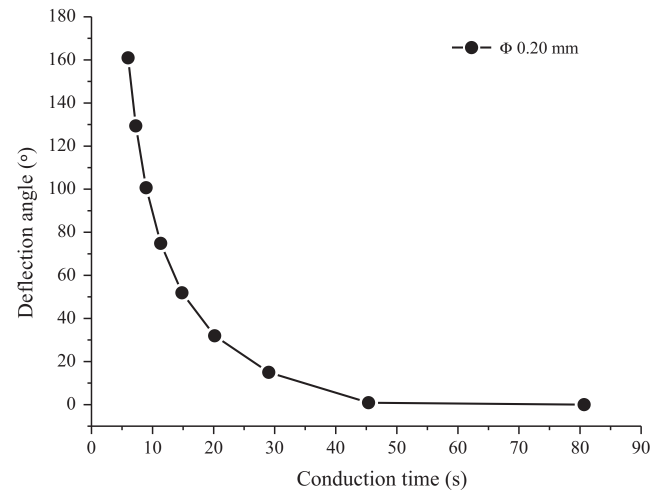

Fig. 10. Relationship between the conduction time and the deflection angle (the diameter of SMA was 0.2 mm and the maximum residual strain was 4%).

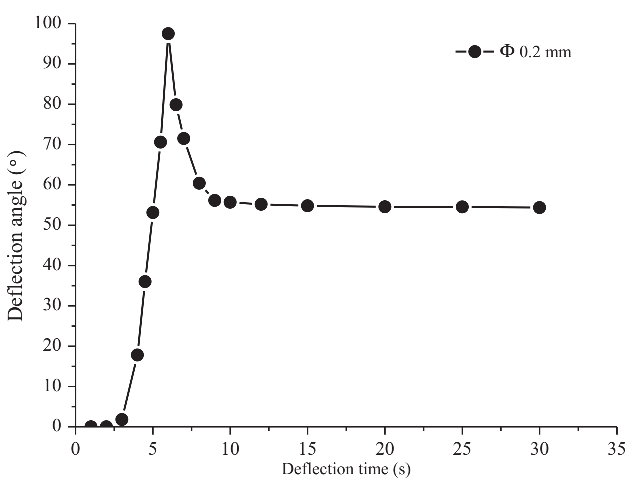

Fig. 9. Relationship between the deflection angle and the deflection time. (The diameter of the SMA wires was 0.2 mm, the maximum residual strain of the SMA wires was 4%, the heating voltage was 8 V, the heating time was 6 s, and the cooling time was 24 s).

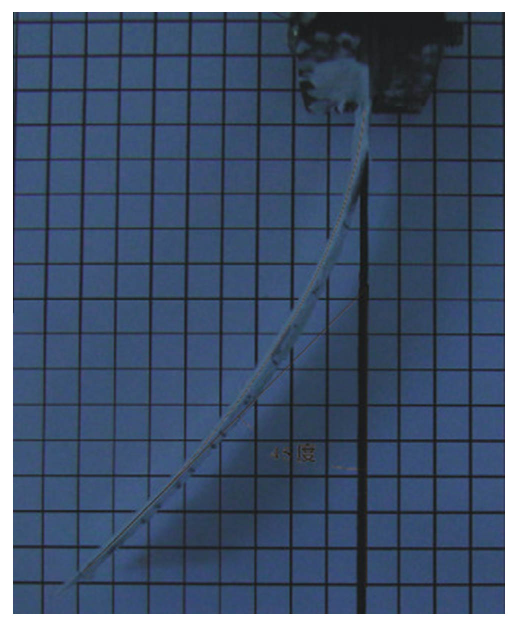

Fig. 11. Prototype of planar bending actuator.

greater deflection angle of the actuator to be obtained. However, it becomes harder for the elastic substrate to recover to the initial state. In this study, a 0.2-mm diameter SMA wire was chosen for the following experiments.

The dynamic bending, which is presented in Fig. 9, indicates that the deflection process can be divided into three stages: no-phase transition stage; phase transition stage; and cooling stage. In the no-phase transition stage, the temperature of the SMA wire increased with time, but did not reach the phase transition temperature. The SMA wires did not provide any driving force, and the deflection angle of the actuator was zero. The duration of this stage is closely related to the heating voltage and the convection heat transfer coefficient. When the temperature of the SMA wire reached the phase transition temperature, the SMA wire began to contract and generated the driving force, the actuator started to bend, and the bending angle increased until the deflection angle reached a maximum value. Finally, the heating current was shut off, and the cooling stage began. The deflection angle of the actuator decreased and remained stable.

We fixed the total heating energy input, which is expressed by $V^2t/R = K$, and varied the heating voltage and time, which are regarded as different heating control strategies. The relationship between the conduction time and the deflection angle is exhibited in Fig. 10. The case of small conduction times but large voltages could generate larger deflection angles, whereas large conduction times with small voltages generated small deflection angles. In addition, when the conduction time is more than 45 s, the actuator could not generate bending. This trend means that the heating strategy play an important role in achieving a larger bending angle. In the current experiments, larger heating voltage with small time yielded optimal results; thus, a pulse heating strategy can perform better.

5. Experimental determination of the actuator characteristics

The prototype of the planar bending actuator embedded with a single SMA wire was developed (Fig. 11). The developed actuator consists of four parts: the SMA wire, the elastic substrate, the surface membrane, and the fixture. To ensure that the properties of the actuators were consistent and possessed stable performances, the manufacture process of the actuators was unified, as shown

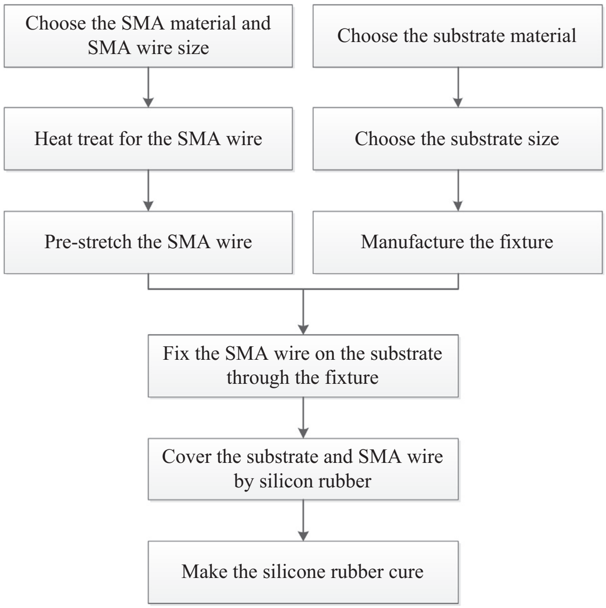

Fig. 12. Process flow chart of the planar bending actuator.

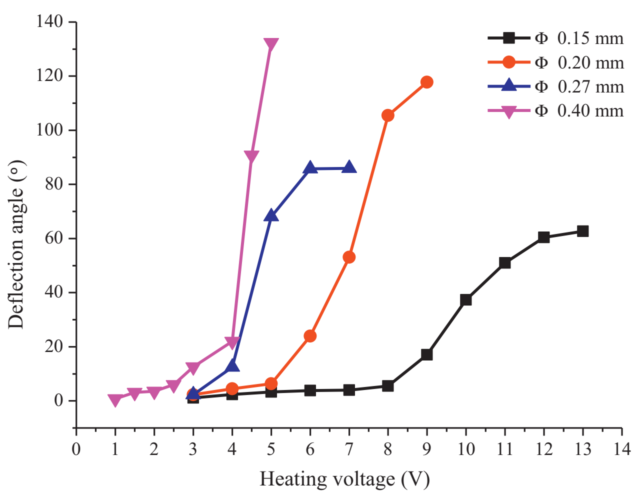

Fig. 13. Relationship between the deflection angle of the planar actuator bending embedded with SMA actuator and the working voltage at different SMA wire diameters (the heating time was 6 s).

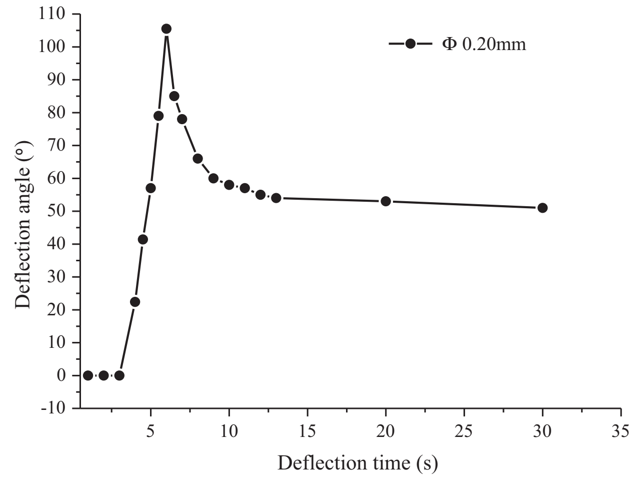

Fig. 14. Relationship between the deflection time and the deflection angle of the planar actuator (the diameter of the SMA wire was 0.2 mm, the voltage was 8 V, the heating time of the SMA wire was 6 s and the cooling time was 24 s.

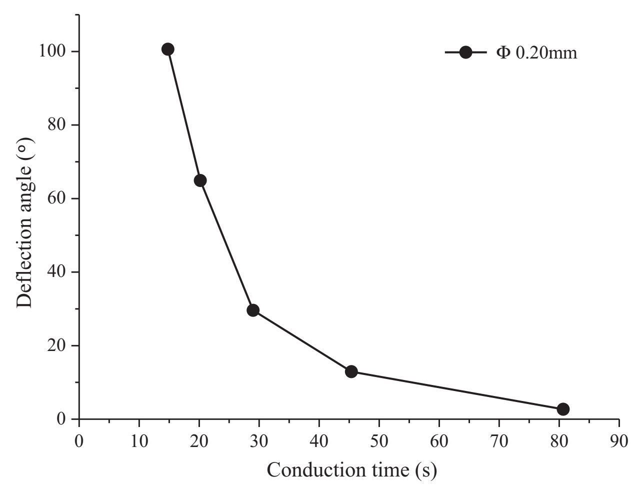

Fig. 15. Relationship between the different conduction time and the deflection angle (the pre-stretching rate was 4% and the diameter of the SMA wire was 0.2 mm).

in Fig. 12. Ni–Ti (50.6%) SMA wires with diameters of 0.15 mm, 0.2 mm, 0.27 mm and 0.4 mm (actual measurement value) were used. The SMA wires were pre-treated to get a stable memory effect by immersion in hot water and cooling in air for 5–10 cycles. The SMA wires were then pre-stretched to 4%. The elastic substrate was made out of polyvinyl chloride (PVC) with the dimensions of 80 mm × 20 mm × 0.32 mm. The SMA wire was fixed to the substrate using the fixture to increase the tension in the wire. A thin membrane, made of Kafuter 704 RTV, was then adhered to the substrate to keep the wire clinging to the substrate while bending. The Kafuter 704 RTV is durable at both high and low temperatures (−60 °C to 250 °C), and can adhere to PVC very well after curing.

Experiments were conducted to evaluate the performance of the planar bending actuators using the same parameters used in the simulation. The influence of various parameters was also investigated. The relationship between the deflection angle and the heating voltage for different SMA wire diameters is shown in Fig. 13. The deflection angle of the planar bending actuator increased along with the heating voltage at a constant diameter. Larger wire diameters also generated larger angles. This trend is consistent with that in the simulation (Fig. 8). However, the differences between them should be noticed. The values obtained for variation in heating voltage at a constant diameter in the experiment are smaller than those in the simulation. The heating voltage of 0.4-mm diameter could go up to 9 V in the simulation, whereas only 5 V in the experiment. The heating voltage of 0.2-mm diameter was observed to be as high as 12 V in the simulation, whereas only 9 V in the experiment. The reason for adopting a lower voltage is to avoid overheating, which could decrease the shape memory effect of the SMA wire. Moreover, the deflection angle in the experiment seemed to remain stable when the voltage was relatively higher. In the experiment, when the heating voltage is too high, the temperature will increase rapidly to reach a large value. However, if the temperature of the SMA wire is too high, the shape memory effect will decrease, and meanwhile the elastic substrates might need to be melted by the SMA wire. This treatment neither leads to an increase or even a decrease in the performance. This phenomenon was not considered in the simulations. Despite the

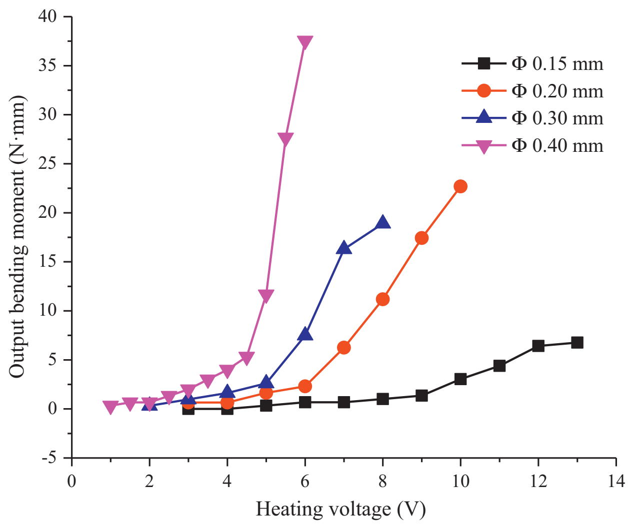

Fig. 16. Relationship between the output bending moment of the planar bending actuator and the heating voltage with different SMA wire diameters (the conduction time was 6 s and the pre-stretching rate was 4%).

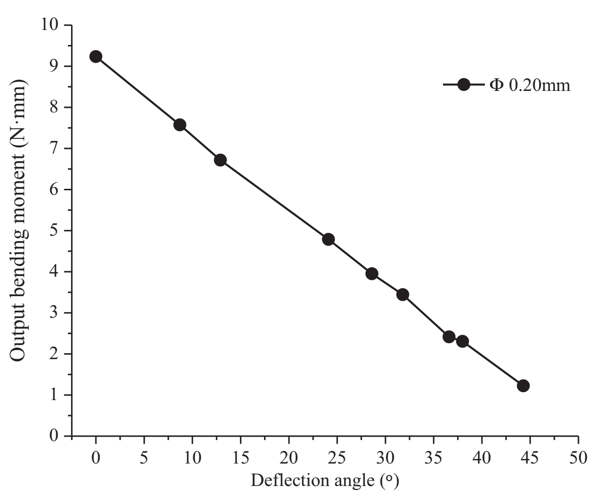

Fig. 17. Relationship between the output bending moment and the deflection angle of the planar bending actuator (the diameter of the SMA wire was 0.2 mm, the heating voltage is 8 V, and the pre-stretching rate is 4%).

differences that exist between the simulation and the experiment, results of the simulation and the experiment were similar for the same diameter and same heating voltage. For example, at a diameter of 0.2 mm, the deflection angle for voltages of 6 V, 7 V, and 8 V were 30°, 61°, and 97.5° respectively, in the simulation, whereas the values obtained were 23.9°, 53.1°, and 105.5°, respectively, in the experiment.

The dynamic response of the actuator is shown in Fig. 14. Results are in accordance with that from the simulation: in the first few seconds, the SMA wire did not yet reach the phase transition temperature, and the deflection angle is zero. When the temperature of the SMA wire reached the phase transition temperature, the actuator started to bend.

The heating strategy had a significant effect on the deflection angle based on the above simulation analysis. We also conduct corresponding experiments as observed in Fig. 15. With the same energy input, a shorter conduction time, and a larger heating voltage, a larger deflection angle can generated. Larger pulse heating strategies could thus generate larger bending angles, and would be useful for the actuator control in practical applications.

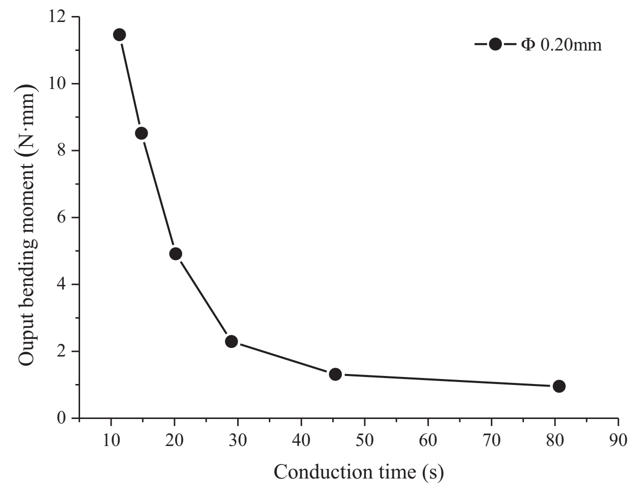

Fig. 18. Relationship between the different conduction time and the output bending moment (the pre-stretching rate was 4% and the diameter of the SMA wire was 0.2 mm).

The bending moment is also a parameter to assess the performance of the planar bending actuator. The relationship between output moment and the heating voltage for different wire diameters is presented in Fig. 16. From the figure, the increase in the SMA wire diameter yields an increase also in the output bending moment. When the diameter of the SMA wire remained constant, larger heating voltage outputs induced bigger bending moment. The relationship between the deflection angle and the bending moment is exhibited in Fig. 17. The deflection angle and the output bending moment have an approximately linear relationship. The greater the deflection angle is, the smaller is the output bending moment. When the deflection angle was zero, the output bending moment of the actuator was at the maximum value. The output bending moment of heating strategies were also investigated in Fig. 18. At a constant energy input, the longer the conduction time is, the smaller is the output bending moment.

6. Conclusions

In this study, we modeled, developed, and tested a novel planar bending actuator embedded with an SMA wire, which can bend into large deflection angles and yield bending moment. A dynamic theoretical model that incorporated the equilibrium of the SMA wire and the elastic substrate, the constitutive equation, and the thermodynamic equation of the SMA wire was first constructed. Prior to calculation, Experiments were performed to measure the characteristics of the SMA wire and obtain necessary parameters in the simulation. In the simulation, the heating voltage and the effect of the diameter on the deflection angle were assessed. The relationship between the deflection angle and the conduction time were also discussed. The heating strategy was then evaluated by fixing the input energy and varying the heating voltage and conduction time. Large heating voltage with small conduction time was determined to perform better, which would be useful for control of the SMA actuators. Experiments on the planar bending actuator were also conducted to verify the theoretical model. The fabrication of the actuator was first presented, and corresponding experiments were carried out. Results from the experiments, along with those from the simulation, validate the efficiency of the theoretical model.

The developed planar bending actuator embedded with the SMA wire is capable of producing a larger deflection angle and a larger moment, which is useful in biomimetic robots, especially in small and lightweight robots, because of the simple structure. The performance of the actuator can be well predicted and the control of the robot can be easily performed when the theoretical model is applied. However, several limitations in the work should still be addressed for future studies. Several thermodynamic parameters need to be regarded as constants for simplification, such as the heat transfer coefficient. Moreover, because of the limitation of the structure and material properties, the overheating of the SMA wire significantly affects the stability of the actuator performance, which renders the control of the actuator more difficult.

Acknowledgment

This study is supported by the National Natural Science Foundation of China (50975270, 50975269), and the Fundamental Research Funds for the Central Universities of China (WK209 0090002).

References

[1] Chen Z, Shatara S, Tan X. Modeling of biomimetic robotic fish propelled by an ionic polymer–metal composite caudal fin. IEEE/ASME Trans Mechatron 2010:448–59.
[2] Wang Z, Hang G, Li J, Wang Y, Xiao K. A micro-robot fish with embedded SMA wire actuated flexible biomimetic fin. Sens Actuat A: Phys 2008;144:354–60.
[3] Yang K, Gu C. A novel robot hand with embedded shape memory alloy actuators. Proc Inst Mech Eng, Part C: J Mech Eng Sci 2002;216:737–45.
[4] Hartl D, Lagoudas DC. Aerospace applications of shape memory alloys. Proc Inst Mech Eng, Part G: J Aerospace Eng 2007;221:535–52.
[5] Choi S, Lee JJ. The shape control of a composite beam with embedded shape memory alloy wire actuators. Smart Mater Struct 1999;7:759.
[6] Wang Z, Hang G, Wang Y, Li J, Du W. Embedded SMA wire actuated biomimetic fin: a module for biomimetic underwater propulsion. Smart Mater Struct 2008;17:025039.
[7] Wang Z, Wang Y, Li J, Hang G. A micro biomimetic manta ray robot fish actuated by SMA. IEEE Int Conf Robotics Biomimetics 2009:1809–13.
[8] Yan Q, Wang L, Liu B, Yang J, Zhang S. A novel implementation of a flexible robotic fin actuated by shape memory alloy. J Bionic Eng 2012;9:156–65.
[9] Lin H-T, Leisk GG, Trimmer B. GoQBot: a caterpillar-inspired soft-bodied rolling robot. Bioinspiration Biomimetics 2011;6:026007.
[10] Kim B, Lee S, Park JH, Park J-O. Inchworm-like microrobot for capsule endoscope. IEEE Int Conf Robotics Biomimetics 2004:458–63.
[11] Lagoudas DC, Tadjbakhsh I. Deformations of active flexible rods with embedded line actuators. Smart Mater Struct 1999;2:71.
[12] Lagoudas DC, Bhattacharyya A. Modeling of thin layer extensional thermoelectric SMA actuators. Int J Solids Struct 1998;35:331–62.
[13] Blonk BJ, Lagoudas DC. Actuation of elastomeric rods with embedded two-way shape memory alloy actuators. Smart Mater Strucut 1998;1:771.
[14] Tadjbakhsh IG, Lagoudas DC. Variational theory of motion of curved, twisted and extensible elastic rods. Int J Eng Sci 1994;32:569–77.
[15] Shu SG, Lagoudas DC, Hughes D, Wen JT. Modeling of a flexible beam actuated by shape memory alloy wires. Smart Mater Struct 1999;6:265.
[16] Kim C, Park B-S, Goo N-S. Shape changes by coupled bending and twisting of shape-memory-alloy-embedded composite beams. Smart Mater Struct 2002; 11:519.
[17] Yang K, Modelling CGu. Simulation and experiments of novel planar bending embedded SMA actuators. Mechatronics 2008;18:323–9.
[18] Brison LC, Huang MS, Boller V, Brand W. Analysis of controlled beam deflections using SMA wires. J Intell Mater Syst Struct 1997;8:12–25.
[19] Moallem M. Deflection control of a flexible beam using shape memory alloy actuators. Smart Mater Struct 2003;12:1023.
[20] Lagoudas DC, Tadjbakhsh IG. Active flexible rods with embedded SMA fibers. Smart Mater Struct 1992;1:162.
[21] Tanaka K, Kobayashi S, Sato Y. Thermomechanics of transformation pseudoelasticity and shape memory effect in alloys. Int J Plast 1986;2:59–72.
[22] Liang C, Rogers C. One-dimensional thermomechanical constitutive relations for shape memory materials. J Intell Mater Syst Struct 1990;1:207–34.
[23] Holman J. Heat transfer. Berkshire, England: McGraw-Hill Book Company (UK) Ltd; 1997.